JOURNAL OF GEOPHYSICAL RESEARCH, VOL. 113, D16113, doi:10.1029/2007JD009739, 2008

Observations and simulations of a large-amplitude mountain wave breaking over the Antarctic Peninsula

R. Plougonven,[1] A. Hertzog,[2] and H. Teitelbaum[1]

Received 20 December 2007; revised 7 May 2008; accepted 28 May 2008; published 27 August 2008.

[1] A case study of a large-amplitude orographic gravity wave occurring over the Antarctic Peninsula is presented, based on observations from the Vorcore balloon campaign and on mesoscale numerical simulations. The Vorcore campaign (September 2005 to February 2006) consisted in the flight of 27 superpressure balloons in the core of the Southern Hemisphere stratospheric polar vortex at altitudes of 16–19 km, from September 2005 to February 2006. On 7 October 2005, one of the balloons exploded as it was flying above the Antarctic Peninsula. The observations collected by another balloon that was flying during the same time period above the peninsula suggest the presence of a very intense gravity wave (peak-to-peak amplitude of the order of 25–30 m s^{-1} in zonal and meridional velocity disturbances). The wave packet is likely undersampled in the balloon observations because of its high intrinsic frequency, but the balloon data set is complemented with high-resolution numerical simulations carried out with the Weather Research and Forecast Model. The simulations are validated by comparison with the balloon measurements and show that the wave was breaking in the lower stratosphere at the time and height where the balloon exploded. The simulations highlight several consequences of the mountain wave on the stratosphere: forcing of the mean flow, generation of secondary inertia-gravity waves, and turbulence and mixing. In particular, the momentum fluxes are calculated and are found to compare well with the estimates from balloon measurements. The large values found are likely extreme values, which raises the issue of their representativity. To discuss this, the balloon measurements are used in conjunction with operational analyses to estimate the frequency of such large-amplitude gravity waves, i.e., to provide an estimate of their intermittency.

Citation: Plougonven, R., A. Hertzog, and H. Teitelbaum (2008), Observations and simulations of a large-amplitude mountain wave breaking over the Antarctic Peninsula, *J. Geophys. Res.*, *113*, D16113, doi:10.1029/2007JD009739.

1. Introduction

[2] Internal gravity waves significantly influence the dynamics of the atmosphere on both small and large scales. On global scales, their upward transport of momentum fluxes from the troposphere is essential to understand the middle atmosphere circulation [*Fritts and Alexander*, 2003], particularly in the mesosphere, but also in the stratosphere [*Haynes*, 2005]. On scales of tens of kilometers, gravity waves provide significant fluctuations of wind and temperature which contribute to turbulence and mixing [*Lane et al.*, 2004; *Koch et al.*, 2005], and influence processes that are sensitive to temperature thresholds, such as polar stratospheric clouds [*Buss et al.*, 2004] or dehydration [*Potter and Holton*, 1995]. It is becoming increasingly appreciated that the gravity wave forcing, both in space and time, is very variable [*Fritts et al.*, 2006]. One implication is that this forcing can provide a secondary source of inertia-gravity waves [*Vadas et al.*, 2003]. This variability, which is in part tied to the intermittency of wave sources, is an important factor to determine the time-dependent (and, through nonlinear processes, the time-averaged) response of General Circulation Models to gravity wave forcing [*Bühler*, 2003; *Piani et al.*, 2004].

[3] Specific motivations for the study of gravity waves in high latitudes include their contribution to Polar Stratospheric Clouds and related microphysics [*Dörnbrack et al.*, 2002; *Shibata et al.*, 2003; *Höpfner et al.*, 2006]. The possibility that mountain waves, in particular above the Antarctic Peninsula, contribute locally to PSCs was already highlighted in one of the earliest papers on large-amplitude gravity waves in that region [*Gary*, 1989]. On a larger scale, they are also primarily responsible for the Southern Hemisphere polar vortex temperatures that are much warmer than those implied by pure radiative considerations [*Hamilton et al.*, 1995]. A better representation of gravity waves in General Circulation Models (GCM) would provide a better forcing for the meridional circulation in the stratosphere, and hence very likely contribute to reduce the common "cold pole bias" [*Pawson et al.*, 2000; *Austin et al.*, 2003].

[1] Laboratoire de Météorologie Dynamique, École Normale Supérieure, IPSL, Paris, France.
[2] Laboratoire de Météorologie Dynamique, Université Pierre et Marie Curie, École Polytechnique, IPSL, Palaiseau, France.

0148-0227/08/2007JD009739$09.00

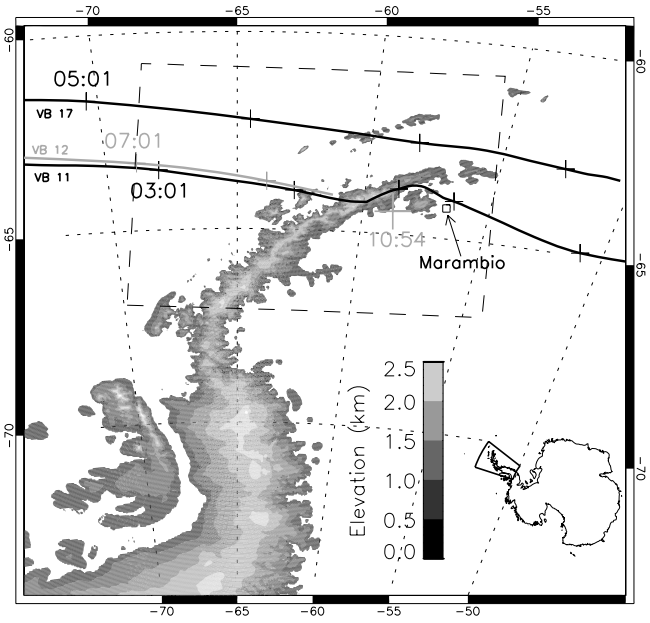

Figure 1. Map showing the topography of the Antarctic Peninsula and the trajectories of Vorcore balloon 11 (black, southern trajectory), Vorcore balloon 12 (grey), and Vorcore balloon 17 (black, northern trajectory) on 7 October 2005. Small crosses are shown every 2 h along the trajectories. The balloons were embedded in the stratospheric, winter westerly flow and therefore traveled from left to right on the figure. The large grey cross on the eastern side of the peninsula indicates the position of VB12 at 1054 UT, when the GPS reported an altitude of 3 km (i.e., after the balloon failure). The small square shows the position of the Argentinian Marambio station. The dashed line delimits the inner domain used in the WRF simulations.

[4] The Vorcore campaign (September 2005 to February 2007), during which 27 long-duration, superpressure balloons were launched in the Antarctic polar vortex, has provided a unique data set to investigate mesoscale motions in the polar and subpolar lower stratosphere, and in particular gravity waves [*Hertzog et al.*, 2007]. Climatologies of momentum fluxes associated with gravity waves have for instance been estimated from these observations [*Vincent et al.*, 2007; *Boccara et al.*, 2008]. In a complementary way, these observations can also be used for case studies that may provide a better understanding of the dynamics and impacts of gravity waves.

[5] In the present study, we focus on a gravity wave event of large amplitude that took place above the Antarctic Peninsula. The first goal that we pursue is to fully characterize the wave packet on the basis of the balloon observations, and in particular to estimate the momentum flux carried by the wave packet. It will nevertheless appear that the wave packet is somewhat undersampled in the balloon observations, so that high-resolution mesoscale simulations using the Weather Research and Forecast model (WRF [*Skamarock et al.*, 2005]) were designed to obtain a more comprehensive view of the wave packet, its generation and evolution. Mesoscale models have indeed proved to be very useful to study mountain waves [e.g., *Broad*, 1996; *Beau and Bougeault*, 1998]. Recently, two cases of large-amplitude mountain waves comparable in many respects to the event studied in this article have been described over Greenland [*Shapiro et al.*, 2005; *Limpasuvan et al.*, 2007]. A second goal of this study is to show that the numerical simulations succeed in reproducing a large-amplitude gravity wave with characteristics similar to those found in the balloon observations. Validating mesoscale simulations, and especially the simulated momentum fluxes, is of great importance, as mesoscale models are believed to be a useful tool to provide constraints on gravity wave drag parameterizations.

[6] The numerical simulations will stress that the wave is breaking through static instability in the lower stratosphere. This provides a significant forcing of the mean flow, which can be quantified from the calculation of the momentum fluxes, but also induces turbulence and mixing at these heights. Such effects, which are associated with a particularly intense gravity wave, are expected to be very intermittent. The last part of the article is thus devoted to a coarse assessment of the probability of occurrence of such large-amplitude mountain waves over the Antarctic Peninsula. Indeed, as case studies generally focus on particularly large and identifiable events, it is worthwhile to estimate how frequent or representative the events studied are.

[7] The paper is organized as follows: the balloon data used are described in section 2. The numerical simulations of the event are described and analyzed in section 3. The significance of this wave event and its impacts are discussed in section 4. Conclusions are presented in section 5.

2. Balloon Data

2.1. Signature of the Wave Packet

[8] The twelfth Vorcore balloon (hereinafter referred to as VB12) was launched on 9 September 2005 from McMurdo, Antarctica. Until 7 October 2005, this balloon was flying nominally at ~50 hPa (~18.5 km) in the lower stratosphere. At 1054 UT on that day, the GPS inside the scientific payload reported an unusually low altitude of 3 km. The following records show further slowly decreasing altitudes, indicating that the flight train had separated from the balloon and was falling under its parachute. Prior to this fall, the last VB12 record in normal flight conditions corresponds to an observation performed by the payload at 1001 UT, and the reported altitude is 19 km. Thus for some reason, VB12 failed between 1001 and 1054 UT on 7 October 2005. (Further inspection of the housekeeping data shows that VB12 flight train crossed the 100-hPa level at 1032 UT, which generally occurs a few minutes after the balloon failure.)

[9] The trajectory of VB12 during that period as well as that of Vorcore balloon 11 (VB11) are displayed in Figure 1. VB11 and VB12 were flying closely together on 7 October, VB11 leading VB12 by about 4 h. As shown by Figure 1, the last position of VB12 in normal flight condition is located on the western side of the Antarctic Peninsula (i.e., just before VB12 crossed the peninsula), whereas the low-altitude records are located on the other side. While none of the data recorded by VB12 when it was crossing the peninsula were received by ground stations, the observations performed by VB11 a few hours earlier at the same

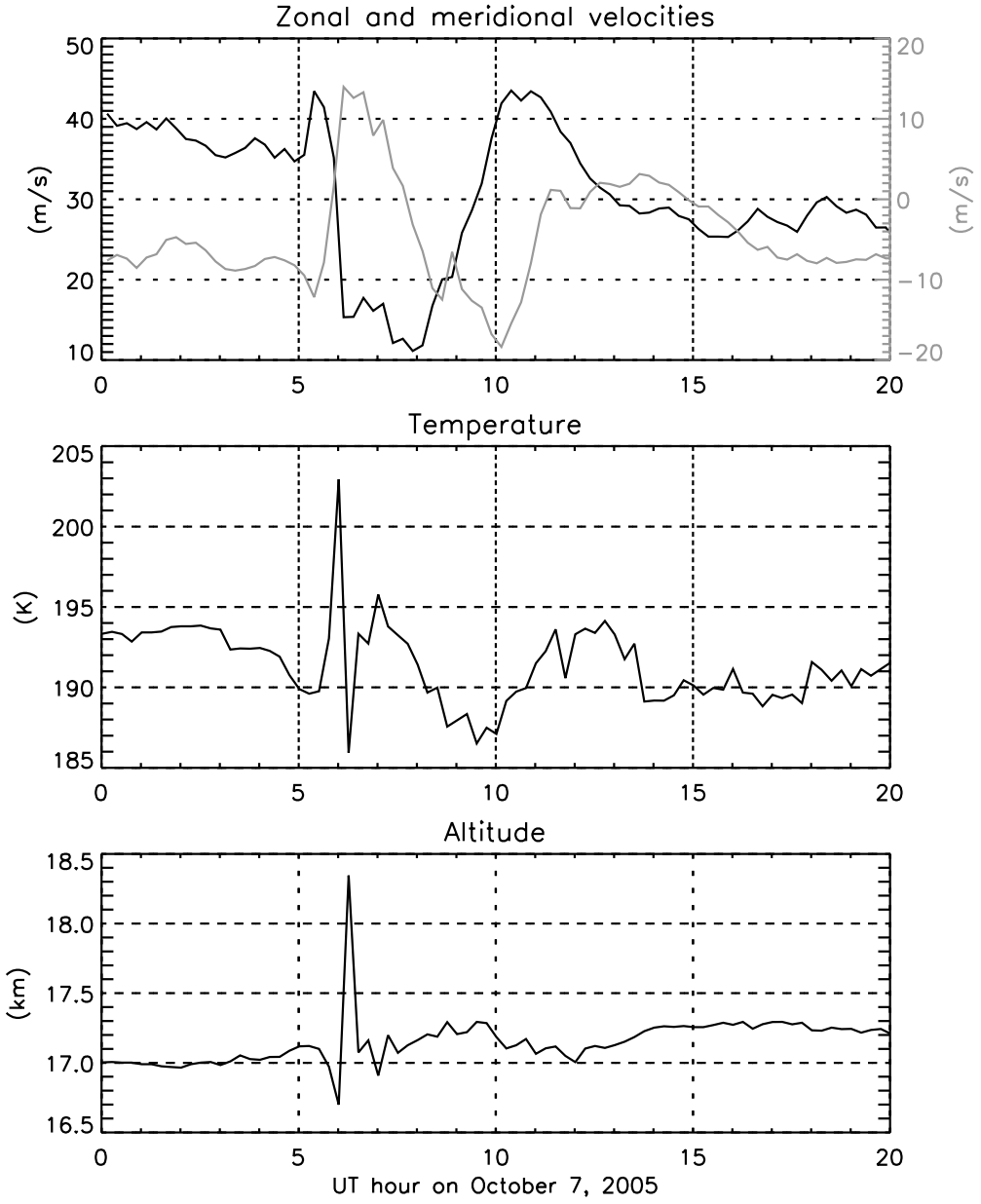

Figure 2. (top) Time series of zonal (black) and meridional (grey) velocities, (middle) temperature, and (bottom) altitude recorded by VB11 on 7 October 2005.

place are available. Because of its smaller size (diameter of 8.5 m, instead of 10 m), VB11 was flying 2 km lower than VB12, but VB11 observations are still useful to understand the reason for VB12 failure.

[10] VB11 horizontal velocities, temperature and altitude on the morning of 7 October are displayed in Figure 2. At the time when this balloon was flying above the peninsula (i.e., ~0600 UT), a sudden and large disturbance is observed on every time series. Peak-to-peak amplitudes in zonal and meridional velocities, temperature, and altitude amount to 30 m s^{-1}, 25 m s^{-1}, 17 K, and 1.7 km, respectively. Notice that the disturbances in horizontal velocities also clearly appear in VB11 trajectory just above the peninsula mountain ridge (Figure 1). Observations were performed every 15 minutes along the Vorcore flights, and the rapid oscillations displayed by the time series indicate that the sampling was probably not sufficient to fully resolve the disturbances. Corresponding disturbances are observed in the atmospheric pressure (18 hPa) and in the superpressure of helium inside the balloon (of the same order). Now, the total force due to pressure acting on the balloon envelope scales with the balloon surface, so that smaller balloons like VB11 can withstand larger superpressure than larger balloons. As reported by *Hertzog et al.* [2007], the maximum superpressure observed by VB11 applied to a balloon of the size of VB12 is sufficient to cause the latter to burst, causing the end of the flight. Moreover, VB12 passed above the peninsula during daytime, in contrast to VB11, so that the helium had already started to warm because of daylight, enhancing further the superpressure experienced by the balloon. (One may ask whether the low temperatures encountered may have altered

the elasticity of the balloon skin and contributed to the balloon failure. Technical specifications, experience from other balloons which encountered yet lower temperatures, and the recordings available of the helium temperature for VB11 and VB12 exclude that possibility.) Another interesting feature in the VB11 time series is the observation of longer-period ($\sim$5 h) disturbances occurring just after the rapid fluctuations at 0600 UT. Those longer fluctuations have amplitudes in horizontal velocities that are similar to those of the rapid event, whereas the induced vertical displacements and temperature disturbances are significantly smaller. We will further discuss these longer fluctuations in section 3.5.

[11] Finally, Figure 1 also shows the trajectory of VB17, which was flying on the same day in the same area of VB11 and VB12, about 200 km north of these two balloons. Consequently, VB17 did not fly over the mountain ridge, and its time series only exhibit a weaker signature of the disturbances reported by VB11 (see section 3.3).

2.2. Characteristics of the Mountain Wave in the Observations

[12] From now on, we will interpret the 0600 UT disturbances seen in the balloon time series as caused by a mountain gravity wave packet generated above the peninsula ridge and propagating upward in the atmosphere. This assumption will be further supported by the numerical simulations reported in the following section, but several aspects of the balloon observations obviously argue for such an interpretation.

[13] Since the superpressure balloons used during Vorcore are advected by the wind, they directly observe the intrinsic period of gravity waves. The reported period of the disturbances ($\lessapprox$45 min) is thus within the gravity wave band [*Andrews et al.*, 1987]: at the time and location of the disturbances, the buoyancy and inertial periods amount to 4 min 45 s and 13 h 20 min, respectively. Furthermore, the ratio of the intrinsic frequency of the wave to the inertial frequency is:

$$\frac{\hat{\omega}}{f} \approx 18 \tag{1}$$

so that the wave can be safely considered as a pure gravity wave. Writing each disturbance field as:

$$u' = \mathrm{Re}\left[\tilde{u}\, e^{i(kx+ly+mz-\omega t)}\right] \tag{2}$$

where Re stands for the real part, (k, l, m) for the zonal, meridional and vertical wave numbers, and ω for the ground-based frequency (which is assumed to be positive without loss of generality), the polarization relations for such a wave read [*Fritts and Alexander*, 2003]:

$$\tilde{u} = \frac{k}{l}\,\tilde{v}, \tag{3a}$$

$$\frac{\tilde{T}}{\overline{T}} = -\frac{N^2}{g}\,\tilde{\zeta}, \tag{3b}$$

$$\tilde{\zeta} = -i\frac{\hat{\omega}}{N^2}\frac{m}{k}\,\tilde{u}, \tag{3c}$$

where ($\tilde{u}$, $\tilde{v}$, $\tilde{T}$, $\tilde{\zeta}$) are the wave complex amplitudes in zonal and meridional velocities, temperature and vertical displacement, $\overline{T}$ the background temperature, N the buoyancy frequency calculated from the ECMWF analyses, and g the Earth gravity. The peninsula mountain ridge has a southwest–northeast orientation at the location where the balloons crossed it, so that a mountain wave generated by an eastward wind flowing above this mountain will propagate toward the northwest, that is $l \sim -k > 0$. Equation (3a) therefore implies that there must be a phase opposition between the wave-induced zonal and meridional velocity disturbances, in agreement with the observations (see Figure 2, top). Equation (3b) implies that there must be a phase opposition between the balloon vertical displacement and the temperature disturbance, again in agreement with the observations (Figure 2, middle and bottom). Finally, equation (3c) states that ζ' must lead u' (since u' is in phase opposition with w'), which is also consistent with the balloon observations.

[14] The horizontal wavelength of the wave packet can be estimated by assuming that the mountain wave is at least at first order stationary with respect to the ground. In this case,

$$\hat{\omega} = -k\bar{u} - l\bar{v} \sim -k(\bar{u} - \bar{v}) \tag{4}$$

where $\bar{u}$ and $\bar{v}$ are the background zonal and meridional velocities, and where we have assumed that $k \sim -l$, which is supported by the observed similar amplitudes of zonal and meridional velocity disturbances. Identifying $\bar{u}$ and $\bar{v}$ to the observed values of the wind velocities before the peninsula, one obtains: $\bar{u} \sim 35$ m s^{-1} and $\bar{v} \sim -10$ m s^{-1}. The zonal wavelength can then be obtained from equation (4), and is $\lambda_x = 2\pi/|k| \approx 120$ km. (The same value is obtained by estimating λ_x directly on the balloon trajectory). With the previous assumptions, the horizontal wavelength is linked to the zonal wavelength through: $\lambda_h = \lambda_x/\sqrt{2} \approx 85$ km. At the latitude where the balloons crossed it, the width of the Antarctic Peninsula is typically of the order of this value, which furthermore support the generation of the wave packet by the peninsula ridge.

[15] The vertical wavelength (λ_z) of the wave can be inferred from the following polarization relation [*Andrews et al.*, 1987]:

$$|\tilde{w}| = \frac{k^2 + l^2}{mk}\,|\tilde{u}| = \frac{2\lambda_z}{\lambda_x}\,|\tilde{u}| \tag{5}$$

and from the amplitude of the vertical velocity disturbance:

$$|\tilde{w}| = \hat{\omega}|\tilde{\zeta}| \approx 2\,\mathrm{m\,s^{-1}}. \tag{6}$$

[16] Notice that we have considered here that the balloon vertical displacement corresponds to the vertical displacement of the air parcels, although it is generally assumed that superpressure balloons behave as isopycnic tracers, and thus underestimate the wave-induced adiabatic vertical displacements of air parcels [*Massman*, 1978]. *Nastrom* [1980] nevertheless showed that the amplitude of the balloon vertical displacements tends asymptotically to that of air parcels in the limit of high-frequency or large-amplitude waves. The wave that we study obviously falls in the latter

Table 1. Characteristics of the Waves in the Lower Stratosphere (15–20 km) at About 0600 UT on 7 October 2005[a]

	λ_h (km)	λ_z (km)	$\hat{\omega}$	$(\tilde{u}, \tilde{v}, \tilde{w})$ (m s^{-1})	$\tilde{\theta}$ (K)	$-\rho\,\overline{u'w'}$ (Pa)	$\rho\,\overline{v'w'}$ (Pa)
Observations	80	8	18 f	(15, 12.5, 2)	17	$\gtrsim 2$	$\gtrsim 2$
Simulations	50–65	8–10	23 f	(20–25, 15–20, 3–4)	15–20	7–9	7–9

[a]The last two columns indicate extreme values for local averages over one or two wavelengths.

case. The assumption in (6) is therefore justified, though it certainly leads us to slightly underestimate the real vertical displacement of air parcels (and consequently the associated disturbance in vertical velocity). Combining (5) and (6) yields $\lambda_z \approx 8$ km. These characteristics of the wave packet are summarized in Table 1.

[17] Finally, the density-weighted zonal momentum flux averaged over one horizontal wavelength is estimated:

$$\rho_0 \overline{u'w'}^{(\lambda_h)} \approx 0.125 \frac{-15 \times 2}{2} \approx -2\,\mathrm{Pa}, \tag{7}$$

where $\rho_0 = 0.125$ kg m^{-3} is the VB11 density level. This value corresponds to the observed peak amplitudes, but because of the wave undersampling in the balloon data set and the assumption made for the balloon behavior, it is likely an underestimate of the real momentum flux. Our momentum flux estimate is typically of the same order (though slightly larger) than values reported in similar mountain wave observations [*Broad*, 1996; *Beau and Bougeault*, 1998; *Shapiro et al.*, 2005]. It is on the other hand significantly larger than the value cited by *Alexander and Teitelbaum* [2007] (0.14 Pa), who studied a mountain wave event at the same location but at much higher altitudes (40 km), making the two situations hardly comparable.

2.3. Radiosounding Downstream of the Peninsula

[18] A radiosounding was launched from the station of Marambio (located just downstream of where VB12 failed, 64.23°S, 56.72°W, see Figure 1) on 7 October at 1100 UT. Measurements were recorded every 2 s (roughly every 10 m), but unfortunately the wind measurements failed, and hence we only show vertical profile of potential temperature (Figure 3). This profile is very significantly disturbed in the stratosphere, showing several conspicuous regions that are fairly well mixed (in particular between 13.5 and 14.5 km, between 15 to 17 km, and again near 23–24 km and 26–27 km). In addition to the balloon observations, the profile therefore suggests that the mountain wave was breaking in several places in the lower stratosphere. This sounding will be further discussed in the light of the numerical simulations in section 3.5.

3. Numerical Simulations

[19] In this section, we first report on the meteorological synoptic situation in the vicinity of the Antarctic Peninsula at the time when the Vorcore balloons were passing by (section 3.1). We then describe the numerical mesoscale simulations that were carried out to provide further details on the dynamical processes that took place over the peninsula on 6 and 7 October 2005 (section 3.2). The numerical outputs are next compared with the balloon measurements (section 3.3). The characteristics of gravity waves generated in the model are detailed in section 3.4, and section 3.5 lastly discusses wave breaking in the simulations.

3.1. Synoptic Conditions

[20] The synoptic meteorological situation in the lower troposphere (850 hPa) in the vicinity of the Antarctic Peninsula is described on the basis of the ECMWF operational analyses and 3-h forecasts. It is displayed in Figure 4 from 6 October 2005, 1500 UT, until 7 October, 1500 UT. On 6 October, a low-pressure system is located on the west of the peninsula at about 100°W, 65°S. This system is associated with a wide area of strong westerly winds (values greater than 20 m s^{-1}) on its western and northern (i.e., equatorward) sides. On 7 October, 0300 UT, the low-pressure center has moved eastward, and is now located at about 85°W, 65°S. The jet region is mainly located on the northern side of the trough (70°W, 60°S), and northwesterly winds begin to blow over the peninsula. Twelve hours later,

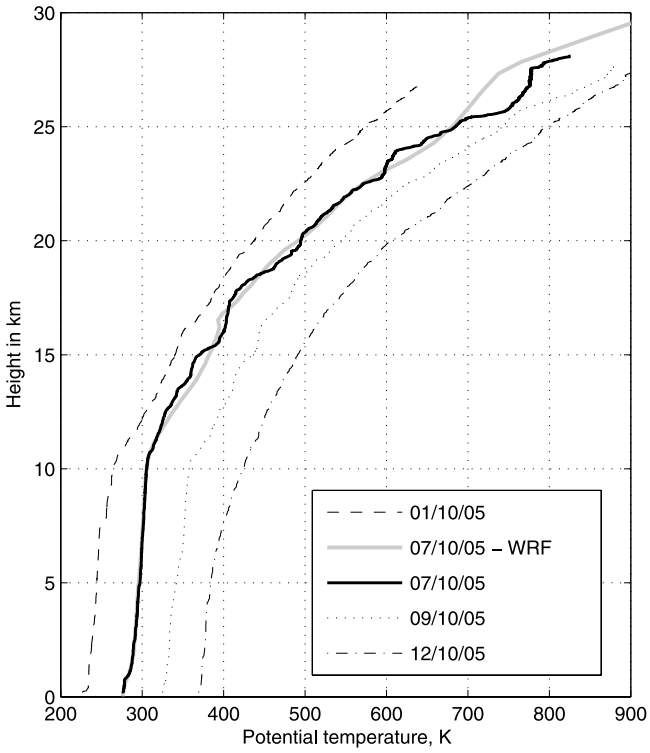

Figure 3. Vertical profiles of potential temperature taken from radiosoundings launched from Marambio on 7 October (solid line) and also on 1, 9, and 12 October (dashed lines, displaced by −50, +50 and +100K, respectively) for comparison. Also shown, in grey, is the vertical profile of potential temperature from the WRF simulation, above Marambio, for 7 October 1200 UT.

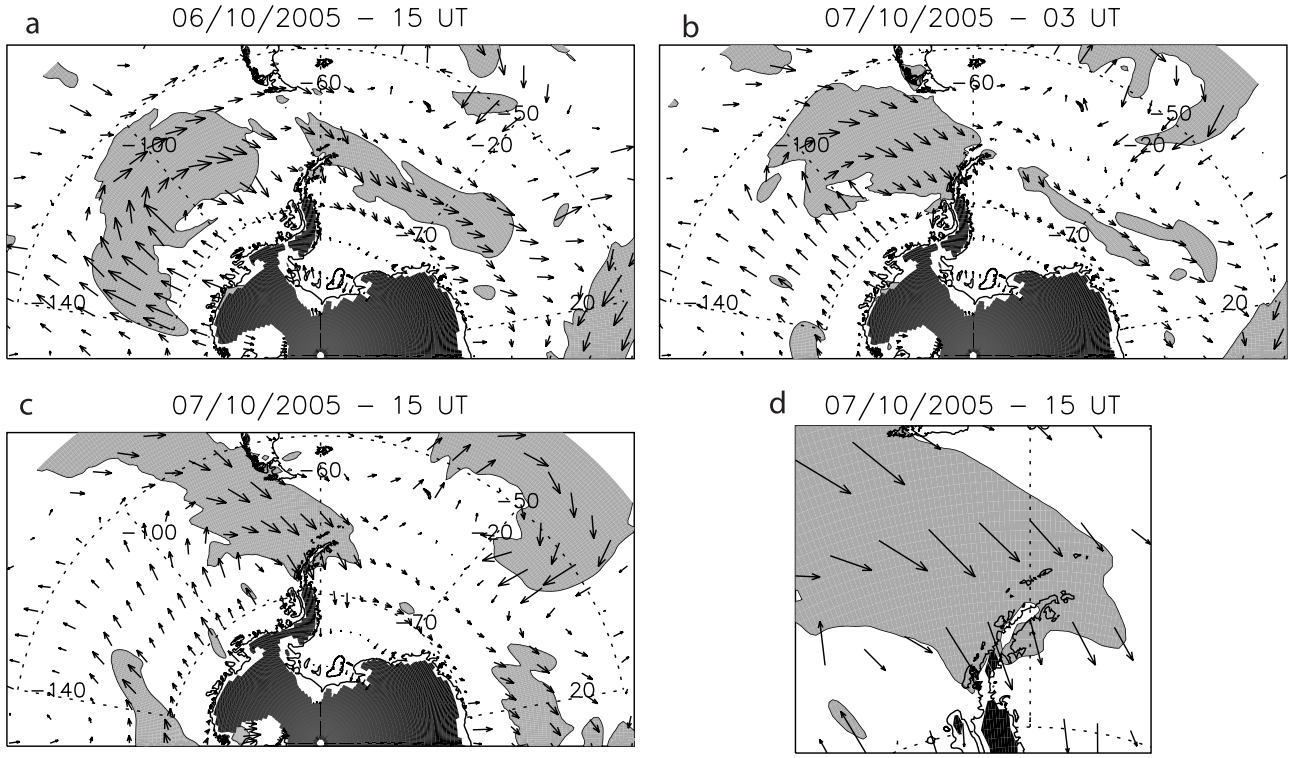

Figure 4. (a–c) Horizontal winds from 3-h forecasts of the ECMWF operational model on the 850-hPa surface. Hours are indicated above each plot. Grey shading corresponds to areas where the modulus of the horizontal wind is greater than 20 m s^{-1}. Regions where the 850-hPa isobar is below the surface are shaded in black. (d) A close-up of the Antarctic Peninsula from Figure 4c.

the low pressure center has moved ~5° further eastward, and the peninsula is now hit by strong winds blowing from the northwest, i.e., almost perpendicular to the mountain ridge. VB11 and 12 were passing over the peninsula on the morning of 7 October, exactly at the time when the winds associated with this low-pressure system reached the mountains. Strong winds keep blowing over the peninsula until the end of 7 October, as the low is further displaced eastward. Yet, the winds now have a more pronounced southward component, and the strongest flow is located on the northern tip of the peninsula. A mountain wave above the peninsula is visible in the ECMWF analyses, but because of their coarse resolution the wavelength is overestimated, and the amplitude is severely underestimated (Figures 8 and 9). The drag exerted by the peninsula on the tropospheric flow is already visible in the ECMWF analyses displayed in Figure 4. When looking closely at the low-level wind pattern in the vicinity of the peninsula (Figure 4d), a region of weaker winds is clearly seen right above the peninsula. To investigate in detail the interaction between the atmosphere and the surface, mesoscale simulations have been carried out and are described below.

3.2. Overall Description of the Simulations

[21] The mesoscale simulations were carried out with the Weather Research and Forecast Model (WRF) [*Skamarock et al.*, 2005], which solves the nonhydrostatic, compressible equations for the atmosphere. We used a two-way nesting configuration (the inner domain is shown in Figure 1), so that the small-scale dynamics in the nested domain acts on the outer domain. Standard parameterizations were used, including the WRF single-moment 3 class for microphysics and the Yonsei University scheme for the planetary boundary layer [*Skamarock et al.*, 2005]. The horizontal spacing is 21 km in the outer domain and 7 km in the inner domain. There are 112 levels from the ground to 1 hPa, corresponding to an altitude of about 42 km. The vertical spacing is about 300 m up to an altitude of about 20 km, except near the ground where the resolution is enhanced. The spacing increases progressively in the last 25 levels, to reach more than 1 km in the last 5 levels. A sponge layer is included in the uppermost 5 km of the domain by increasing the diffusion in order to avoid having excessive reflection of gravity waves from the model lid. Topography is interpolated from the 30″ database provided with WRF. The model is forced at the initial integration time, and on its boundaries, with the 6-hourly operational analyses from the European Center for Medium-Range Weather Forecasts (ECMWF).

[22] The simulations were started on 5 October, 1200 UT and were run for 54 h until 7 October, 1800 UT. A time-altitude cross section of the horizontal wind upstream of the peninsula is displayed in Figure 5. In agreement with the ECMWF analyses, the wind is continuously increasing on 7 October, and exceeds 25 m s^{-1} in most of the troposphere. The orientation of the winds in the troposphere evolves during the day, but there is continuously a significant wind component perpendicular to the peninsula (more than 20 m s^{-1}), so that meteorological conditions on 7 October clearly favor the generation of mountain waves.

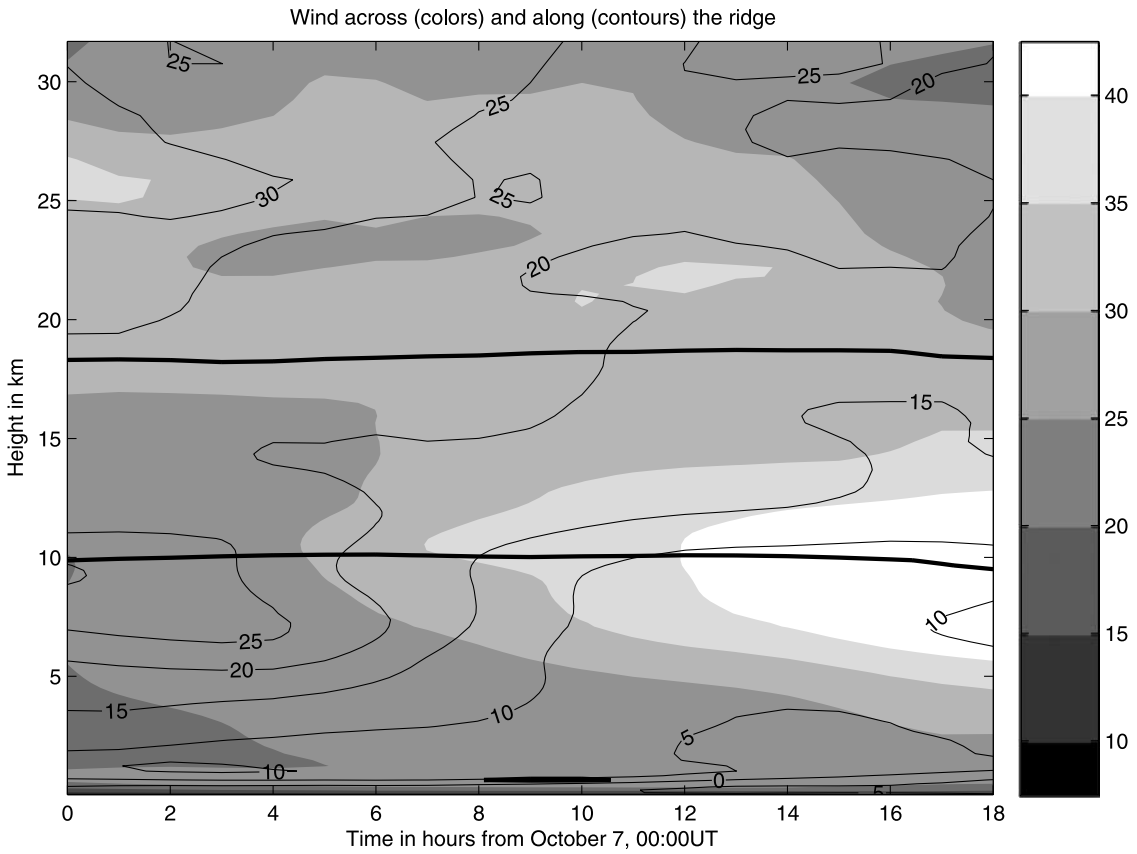

Figure 5. Time-height section of the wind in m s^{-1} upstream of the peninsula in the WRF nested domain on 7 October 2005, from 0000 UT to 1800 UT. The wind has been averaged between 66°S and 58°S, and 65°W and 62°W, but is fairly insensitive to the box chosen. Shading indicates the wind component normal to the ridge (45° clockwise from east), whereas thin lines indicate the wind component parallel to the ridge. In both cases, the contour interval is 5 m s^{-1}. Thick black lines depict two values of the Brunt-Väisälä frequency: N = 1.5 10^{-2} rad s^{-1} (lower line) and 3 10^{-2} rad s^{-1} (upper line).

[23] Another simulation with a different setting was run and compared with the one described below: the model top was set at 10 hPa only, and the simulation was started on 6 October, 1200 UT. The main features of the wave discussed in the present study (characteristics, amplitude, indications of breaking, fluxes) were found to be robust. Nevertheless, differences were found between the two simulations, showing that the precise aspect and parameters of the wave in such mesoscale simulations remains sensitive to the setting of the simulation [*Leutbecher and Volkert*, 2000].

[24] A horizontal cross section of the simulated vertical velocity in the lower stratosphere taken from the nested domain is shown in Figure 6. This field is dominated by a gravity wave developing above the Antarctic Peninsula. Figure 7 furthermore shows vertical cross sections of the vertical and horizontal wind components in the nested domain. Figure 7 highlights that the simulated wave packet is generated by the peninsula ridge and propagates upward in the stratosphere. The isentropes are seen to be severely distorted above the peninsula, and are nearly vertical and overturning in several regions spaced by one wavelength (e.g., around 17–19 km, and again around 26–28 km). Finally, it is noteworthy that, in the lee of the stratospheric wave, layered structures are clearly visible in u and v with large amplitudes, yet essentially absent from w. These will be further discussed in section 3.5.

3.3. Comparison With the Observations

[25] The simulations are compared directly to the balloon observations by interpolating the simulated fields (horizontal wind and temperature) at the balloon locations. This is a quite stringent assessment of the realism of the simulation: for instance, the model may simulate realistic features of the flow but at somehow shifted locations, and the present comparison will then be poorer than deserved. Such direct comparisons thus tend to emphasize the differences between the simulations and the observations. Nevertheless, it appears that the model simulations reproduce reasonably well the balloon observations.

[26] Comparisons are shown for balloon VB11 (Figure 8) and for balloon VB17 (Figure 9). It appears that the model captures very satisfactorily the presence of the wave just above the peninsula, and produces an amplitude that is comparable to the balloon observations. Also shown, for comparison, are the ECMWF fields from the analyses, interpolated at the same locations. The mesoscale features associated to the wave are essentially absent from these, and this makes the benefit of using WRF to study these small-

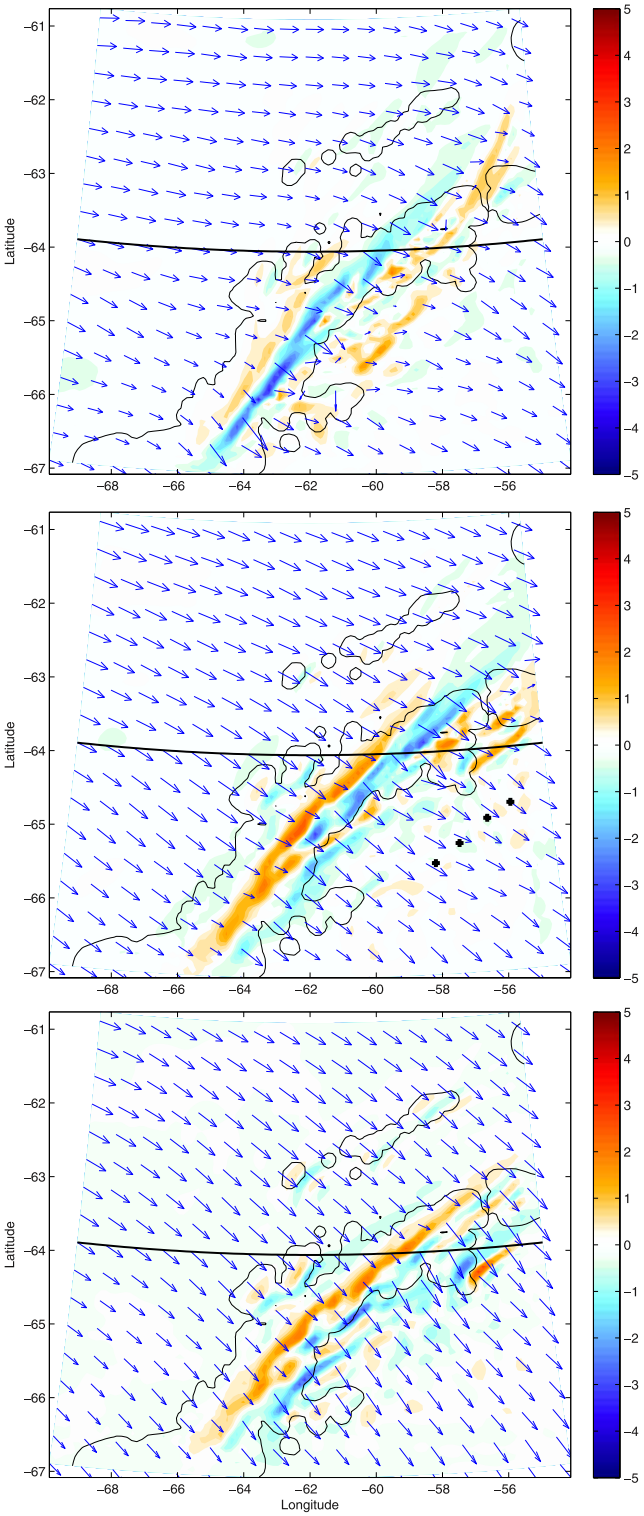

Figure 6. Horizontal maps of the vertical velocity in m s^{-1} and of horizontal wind at altitude z = 15 km, for 7 October 2005, (top) 0300 UT, (middle) 0900 UT, and (bottom) 1500 UT, in the nested domain. The line shows the location of the vertical cross sections of Figure 7, and the crosses in Figure 6 (middle) indicate the location of the soundings of Figure 11.

scale features evident. On the other hand, the model has more difficulties to accurately simulate the flow in the lee of the peninsula. This is understandable as the flow in the lee of the peninsula results in part from the forcing due to the wave and its breaking. As this breaking cannot be properly resolved in the simulations, we do not obtain as good an agreement between the observed and simulated fields as for the mountain wave itself.

3.4. Characteristics of the Wave in the Simulations

[27] In this section, we give further details on the characteristics of the gravity wave packet in the simulations, as was done with the balloon observations. In the following, the characteristics of the wave are estimated in the nested domain.

[28] In the simulated fields, graphical estimation of the horizontal wavelength typically yields $\lambda_x \sim 80-100$ km in the zonal direction, $\lambda_y \sim 70-90$ km in the meridional direction, yielding a wavelength of $\lambda_h \sim 50-65$ km in the southeast direction, i.e., perpendicular to the mountain. The vertical wavelength is about $\lambda_z \sim 10-12$ km in the troposphere, $\lambda_z \sim 8-10$ km in the stratosphere. Such values in the lower stratosphere yield an intrinsic frequency $\hat{\omega} \sim (3.0 \pm 0.5) \times 10^{-3}$ rad s^{-1} $\sim 23 \pm 3.5$ f, or an intrinsic period $\hat{T} \sim (35 \pm 5)$ min. Hence the wave can well be approximated as a pure internal gravity wave. These estimations of the wavelength, direction of propagation, and intrinsic frequency are in very good agreement with the balloon measurements, see section 2 and Table 1.

[29] One can also calculate the intrinsic frequency by assuming that the wave is nearly stationary with respect to the ground, as suggested by Figures 6 and 7. Thus, $\hat{\omega} = k_h \bar{u}_\perp$, where the horizontal velocity normal to the ridge ($\bar{u}_\perp$) is typically 30–35 m s^{-1} according to Figure 5. This yields $\hat{\omega} \sim (3.4 \pm 0.3) \times 10^{-3}$ rad s^{-1}. The consistency between the values of $\hat{\omega}$ estimated from the dispersion relation and from the Doppler shift further confirms that the interpretation in terms of gravity wave is fully justified.

[30] The amplitude of the wave-induced disturbances in vertical velocity is estimated directly from the simulated field above the peninsula. In that region, the mountain wave actually accounts for most of the vertical velocity fluctuations (see Figure 7). At stratospheric heights comparable to those of the balloons, we find that $|\tilde{w}| \sim 3-4$ m s^{-1} in the nested domain. Similarly, other cross sections indicate amplitudes of $\sim$20–30 m s^{-1} for the horizontal velocity disturbances ($\tilde{u}_\perp$) in the direction perpendicular to the mountain ridge, and of $\sim$15–20 K for the potential temperature disturbances ($\tilde{\theta}$). These values are fully consistent with the values estimated from the balloon observations. They are also consistent with values that can be estimated from the wave characteristics: for example, injecting $\lambda_h \sim 60$ km, $\lambda_z \sim 8$ km, $\hat{T} \sim 40$ min into the polarization relation that relate $\tilde{u}_\perp$ and $\tilde{\theta}$ to $\tilde{w} \approx 3$ m s^{-1} yields

$$|\tilde{u}_\perp| = \frac{\lambda_h}{\lambda_z}|\tilde{w}| \sim 22.5\,\mathrm{m\,s^{-1}}, \quad |\tilde{\theta}| = \frac{\theta_0 N^2 \hat{T}}{2\pi g}|\tilde{w}| \sim 16\,\mathrm{K}, \qquad (8)$$

where θ_0 is the background potential temperature. The quoted values therefore correspond to a very large amplitude gravity wave event. *Shapiro et al.* [2005] reported of a similar event above Greenland, and furthermore showed that

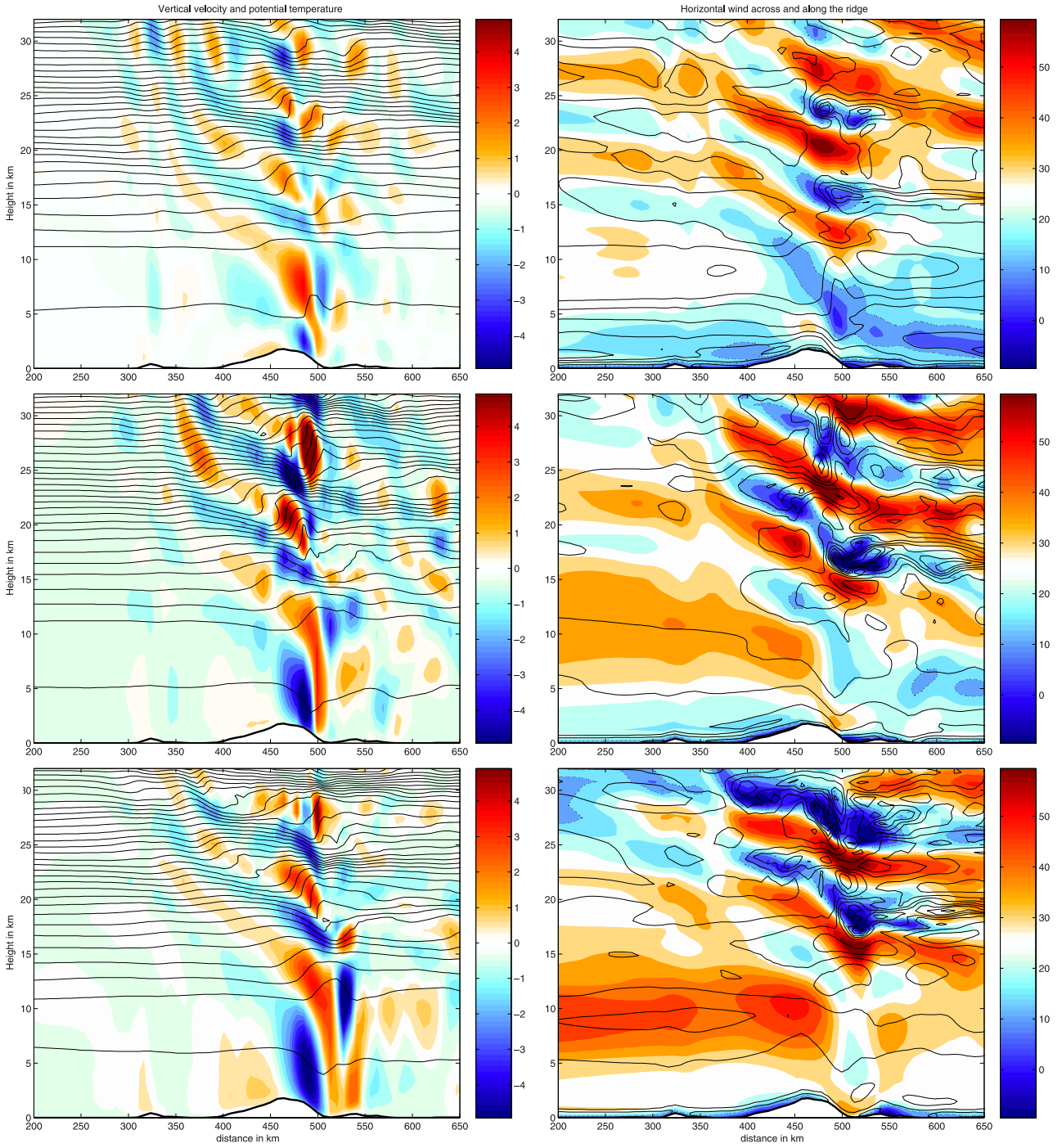

Figure 7. Vertical cross sections of (left) vertical velocity (in m s^{-1}, colors) and potential temperature (contours) and (right) horizontal wind (colors for u, contours every for v, contour interval 5 m s^{-1}). The cross sections are taken along the line shown in Figure 6. Times displayed are 7 October 2005, (top) 0300 UT, (middle) 0900 UT, and (bottom) 1500 UT.

the wave was breaking in their simulations. This is also the case with our simulations, as is now shown.

3.5. Wave Breaking

[31] Given the characteristics and amplitude of the wave found above, the wave-induced maximum vertical gradients of potential temperature in the lower stratosphere are sufficient to induce regions of static instability (we have $(2\pi/\lambda_z)\,(g/\theta_0)\,\tilde{\theta} \sim 5 \times 10^{-4} s^{-1}$). This is illustrated in Figure 7, where isentropes become nearly vertical in several regions in the stratosphere. A further confirmation is obtained by diagnosing the Richardson number $Ri = N^2/|d\mathbf{u}/dz|$ from the simulations: Figure 10 shows that in a large region of the flow above the peninsula the isentropes are overturning at the time when balloon VB12 was flying over the peninsula. It also makes clear the contrast between

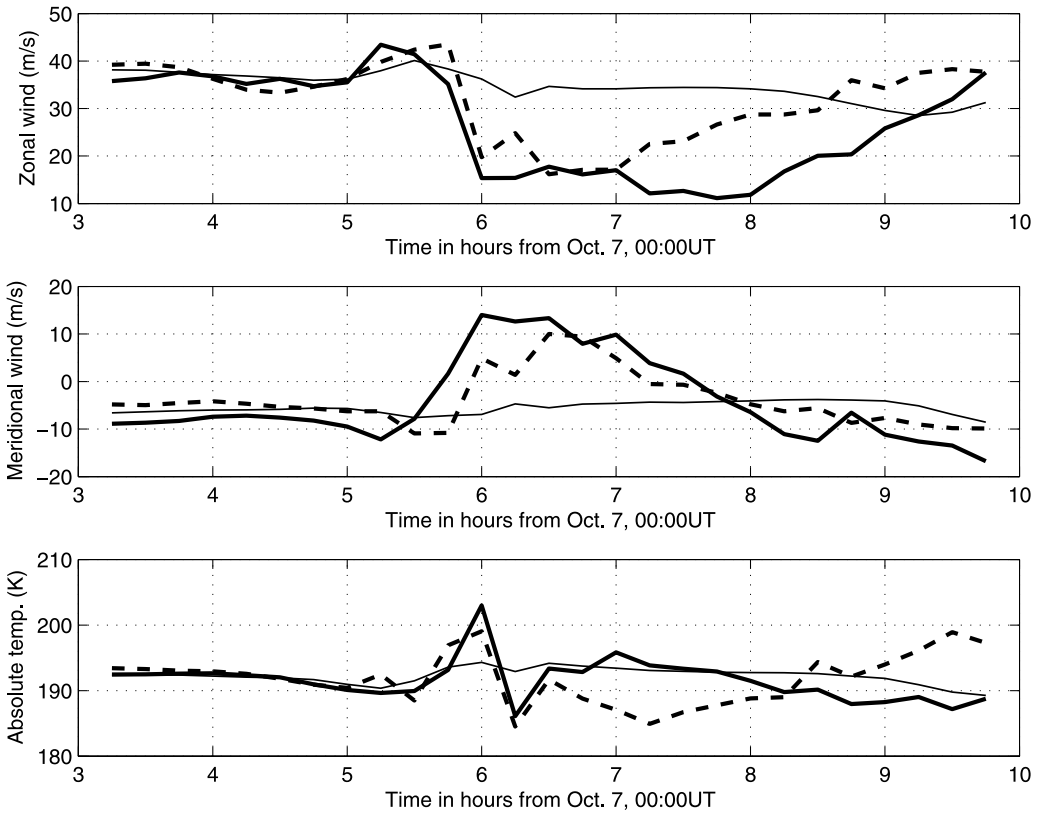

Figure 8. Comparison of u, v, and temperature as functions of time, from the measurements of balloon VB11 (solid line), from the simulations (dashed) in domain 2, and from the ECMWF (thin).

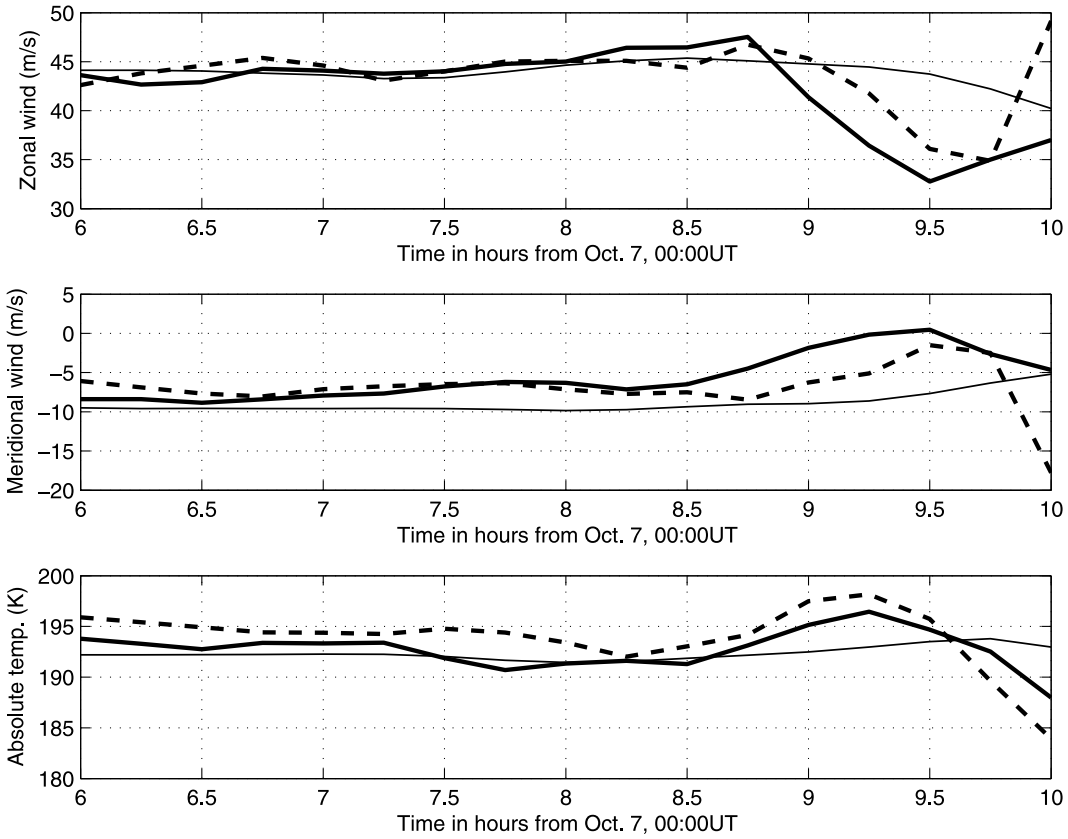

Figure 9. Same as Figure 8 but for balloon VB17.

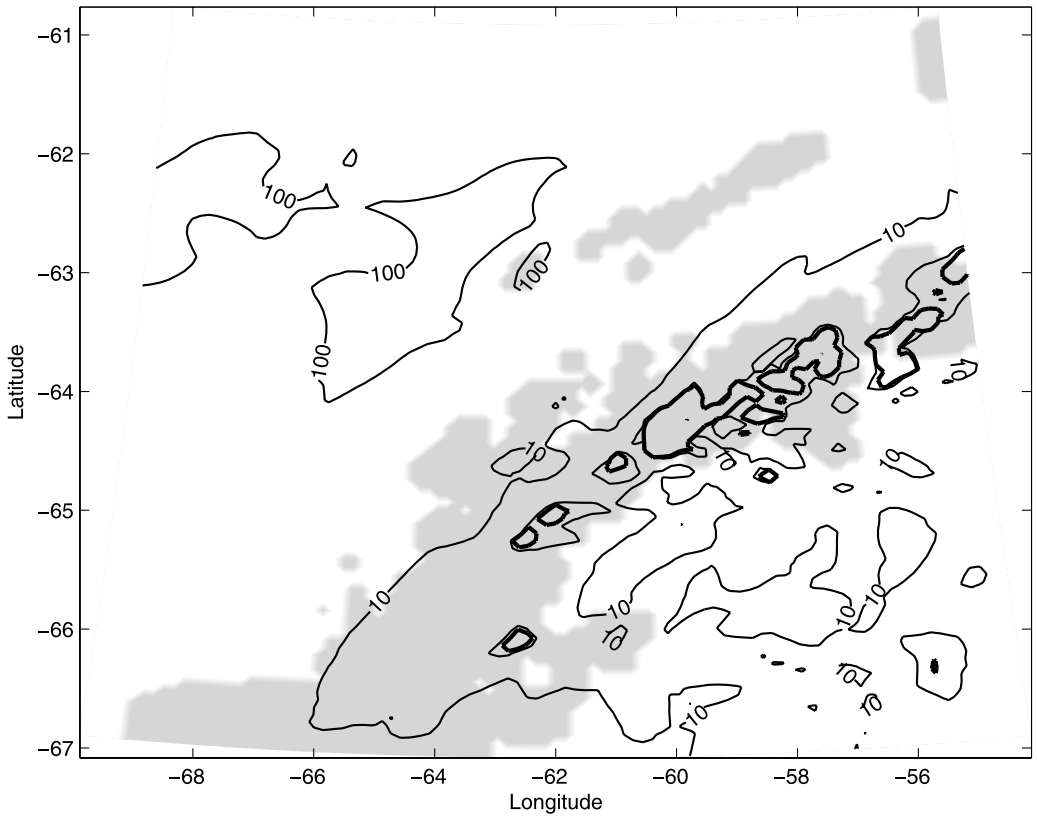

Figure 10. Map of the minimum Richardson number in the altitude range 12–20 km, from domain 2 on 7 October 2005, 0900 UT. The thick contour outlines regions of static instability ($Ri < 0$). Other contour lines indicate Ri values of 1, 10 (labeled), and 100 (labeled).

the very stable conditions upstream ($Ri_{min} > 10$ and even $Ri_{min} > 100$) and downstream of the peninsula ($Ri_{min} < 10$ at most locations). Inspection of the simulations reveals that there is continuous breaking during the time period investigated (7 October 2005, 0000–1800 UT). Finally, note that the cross sections of horizontal velocity (Figure 7) suggest that the wave is also inducing severe winds downslope of the mountain. This may account for the significant reduction in vertical momentum fluxes in the first kilometers of the troposphere, see section 4.1.

[32] Given that the amplitudes of the wave in the simulations and in the observations are comparable, the presence of significant regions of static instability in the model simulations provides evidence that the wave was breaking in the lower stratosphere at the time when VB12 was flying over the peninsula. Though not necessary to explain the explosion of VB12, the breaking has very likely contributed to the vertical motion of the balloon and hence its explosion.

[33] The breaking of the wave in the lower stratosphere has several important implications:

[34] 1. The analysis of the potential temperature in the sounding from Marambio (Figure 3, section 2.3) shows clearly that several layers have been thoroughly mixed, nearly homogenized, in particular between 15 and 17 km. This is evidence for the presence of turbulence upstream of the radiosounding, i.e., where the gravity wave is breaking. The comparison of the potential temperature in WRF and in the sounding shows that the simulation carries relevant indications of this mixing in the lower stratosphere (around 16 km), though the mixed layers above 20 km are not found. Moreover, as could be expected, the model underestimates the homogenization of layers in which the wave breaking has occurred.

[35] 2. The forcing associated with the breaking wave is very localized in space and time, and as such it will act as a secondary source of inertia-gravity waves [*Scavuzzo et al.*, 1998; *Vadas et al.*, 2003]. The layered structure found in both components of the horizontal wind, but absent from the vertical wind, downstream of the mountain wave in the stratosphere (Figure 7) appears to correspond in part to inertia-gravity waves. Further evidence that these oscillations in u and v correspond to inertia-gravity waves comes from the inspection of hodographs of the wind in the lower stratosphere downstream of the mountain (Figure 11): these show distinct ellipses with aspect ratios of about 2 to 3, and always rotating anticlockwise with height. This is indication of inertio-gravity waves with frequencies of the order of $2–3f$ and propagating upward. The vertical wavelengths found are 5–7 km, which is typical for such waves [*Sato*, 1994].

[36] This evidence for secondary generation of IGWs is in agreement with the balloon measurements, which have shown an enhanced presence of IGWs in the lee of large-amplitude mountain waves. This secondary source of IGWs is expected to exist on theoretical grounds [*Scavuzzo et al.*, 1998; *Fritts et al.*, 2006], but has seldom been documented in observations and simulations. A more detailed comparison with the observations, however, is beyond the scope of

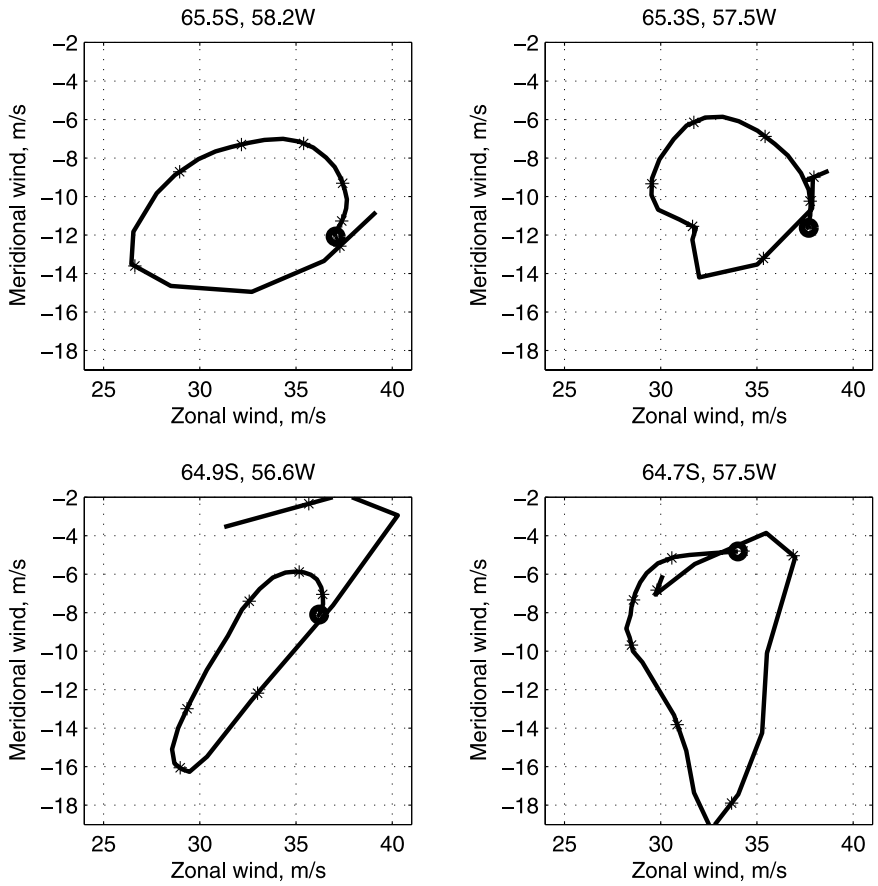

Figure 11. Hodographs of vertical profiles of u (horizontal axis, in m s^{-1}) and v (vertical axis), taken from the model output for 7 October, 0900 UT, at locations as indicated in Figure 6. The starting point of the hodograph is indicated by a large dot, and heights are indicated by marks every km from 12 to 19 km.

the present study, the present numerical simulations being limited by the size of the domain used.

[37] 3. The divergence of the momentum flux associated with the mountain wave contributes to the forcing of the stratospheric circulation on large scales, as is further discussed in the next section.

4. Discussion

[38] The previous sections have shown that the numerical simulations compare reasonably well with the observations. Below we use those simulations to discuss two issues related to this large-amplitude wave event, namely the momentum fluxes associated with this wave (section 4.1) and the frequency of such large-amplitude events (section 4.2).

4.1. Momentum Fluxes Toward the Stratosphere

[39] It is known that estimates of momentum fluxes are very sensitive to resolution, as has been documented for example by *Smith et al.* [2006]. Hence, before using our simulations to estimate momentum fluxes, it is essential to note the agreement found above in the comparison of the observations and the simulations. This suggests that our simulations have a sufficient resolution to be used for the following discussion.

[40] The momentum fluxes associated with this wave event can be estimated in two ways: (1) from the estimate of the amplitude and characteristics of the wave, obtained either from the observations or from the numerical simulations, and (2) by direct calculation and integration from the simulation output. The comparison of the two will provide insight regarding the validity of the assumptions made in analyzing the Vorcore data.

[41] From the estimates of wave amplitudes ($|\tilde{u}_\perp| \sim 25$ m s^{-1}, $|\tilde{w}| \sim 3$ m s^{-1}, where $u'_\perp = (u' - v')/\sqrt{2}$) and from the density value at the flight level of VB11 ($\rho_0 \sim 0.125$ kg m^{-3}), we obtain local values of the density-weighted momentum flux ($\overline{\rho u'_{perp} w'} = \frac{1}{2}\rho|\tilde{u}_\perp|\,|\tilde{w}|$) that reach $\sim$5 Pa.

[42] To estimate momentum fluxes directly from the simulations, anomalies were obtained by removing, at each height, the average over the whole domain at that height: $u' = u - \int\int u\,dxdy / \int\int dxdy$. The momentum fluxes $\rho\,u'w'$ were averaged over squares 140 km $\times$ 140 km (i.e., 20 $\times$ 20 grid points). The size of the boxes was chosen so that they encompass several wavelengths. It is found that the maximal values of momentum flux are very localized and reach 7 to 9 Pa at heights between 15 and 20 km. This is remarkably consistent with the estimate found above simply from the amplitude of the wave.

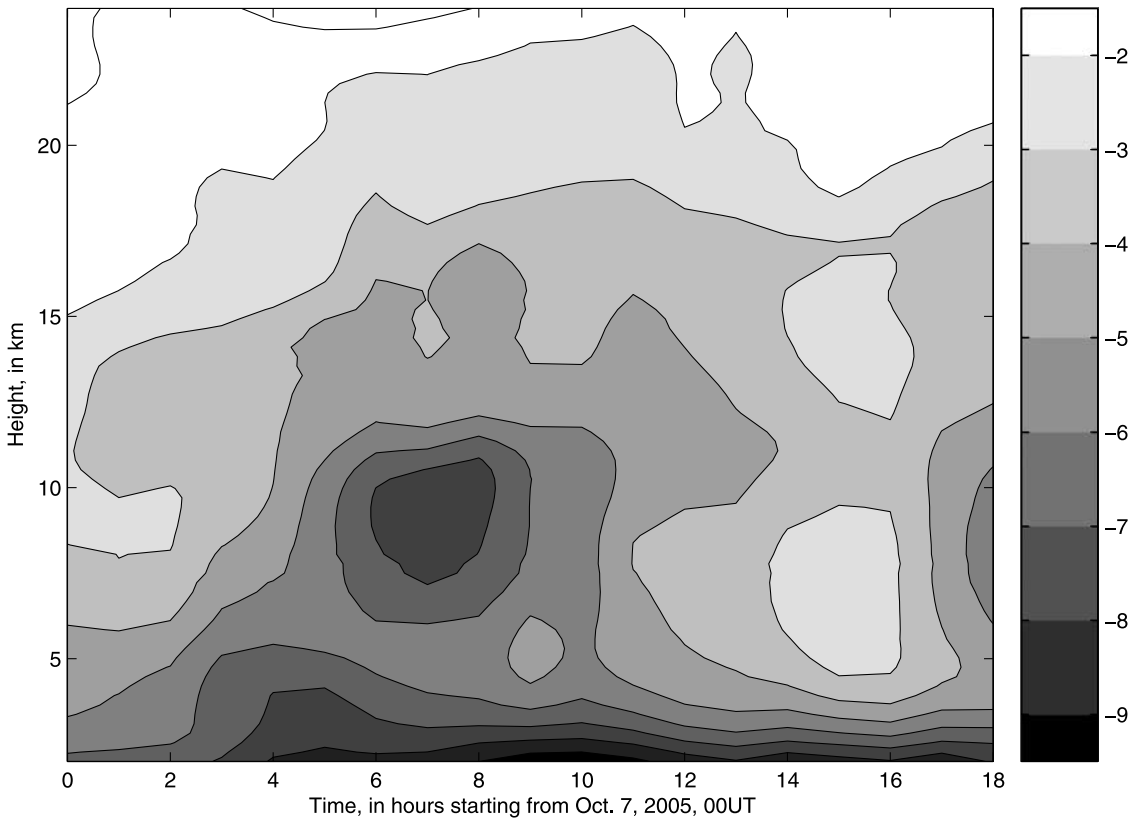

Figure 12. Momentum fluxes in the southeast direction (perpendicular to the peninsula) integrated over the region between 65°S and 62°S, and 64°W and 56°W, for 7 October, 0900 UT. Units are 10^{10} N.

[43] The above estimations however only provide an estimate for the maximum values of $\rho\overline{u'_\perp w'}$. The forcing in the stratosphere, where the wave breaks, will depend on the integral of this term, which is spatially very inhomogeneous. The total flux

$$\mathcal{F}_\perp(z,t) = \int\int \rho u'_\perp w' \, dxdy, \tag{9}$$

was thus calculated over a limited area around the mountain (between 65°S and 62°S, and 64°W and 56°W) and is shown in Figure 12. It was verified that the obtained values are hardly sensitive to the chosen geographical area. In particular, the total flux over the whole nested domain yields values that are only 10% larger than those in the small window defined above, indicating that the mountain gravity wave accounts for most of the flux in the domain. Several points are worth noting. First, the momentum flux decreases sharply in the lower troposphere. This is consistent with the nonlinear phenomena observed in the lower layers from the simulations (downslope windstorm [e.g., *Holton*, 1992]). This decrease is also evident when one compares the drag exerted on the mountain with the values of the momentum flux at low altitudes in the troposphere (Figure 13): at $z = 2$ km, the momentum fluxes are already considerably reduced relative to the surface drag. Second, the momentum fluxes show a second pronounced decrease in the lower stratosphere at the time when the wave is most intense (7 October, 0600 UT to 1000 UT), consistent with the breaking occurring there. The associated deceleration of the mean flow in the lower stratosphere reaches up to 10 m s^{-1} h^{-1} in very localized areas (squares of 140 km by 140 km). Finally, the overall flux increases as the wind increases during the beginning of the period (7 October, from 0000 UT to 0900 UT), and then decreases during the rest of the simulated period.

4.2. Frequency of Such Events During the Vorcore Campaign

[44] The large-amplitude wave event reported in the previous sections illustrates the strong variability of the gravity wave field. Local values of momentum fluxes were found to be very intense, but only in a very limited area and for a limited time. More generally, the intermittency of gravity wave forcing is generally one of the least constrained parameters in gravity wave drag parameterizations [*Alexander and Dunkerton*, 1999], though it significantly influences the altitude where gravity waves break and forces the residual circulation in the middle atmosphere [*Bühler*, 2003; *Piani et al.*, 2004]. Our simulations have for example shown that the large-amplitude wave that we studied already breaks in the lower stratosphere, and so forces the flow at these low altitudes. The impact of such an intense and localized wave is thus very different from that of a series of smaller waves that carry the same momentum fluxes overall, but which could each propagate further up in the atmosphere. A key issue is thus to determine how representative, or how frequent, such large-amplitude gravity wave events actually are. The mountain wave signature in the pressure time series of VB11 (Figure 14) for instance

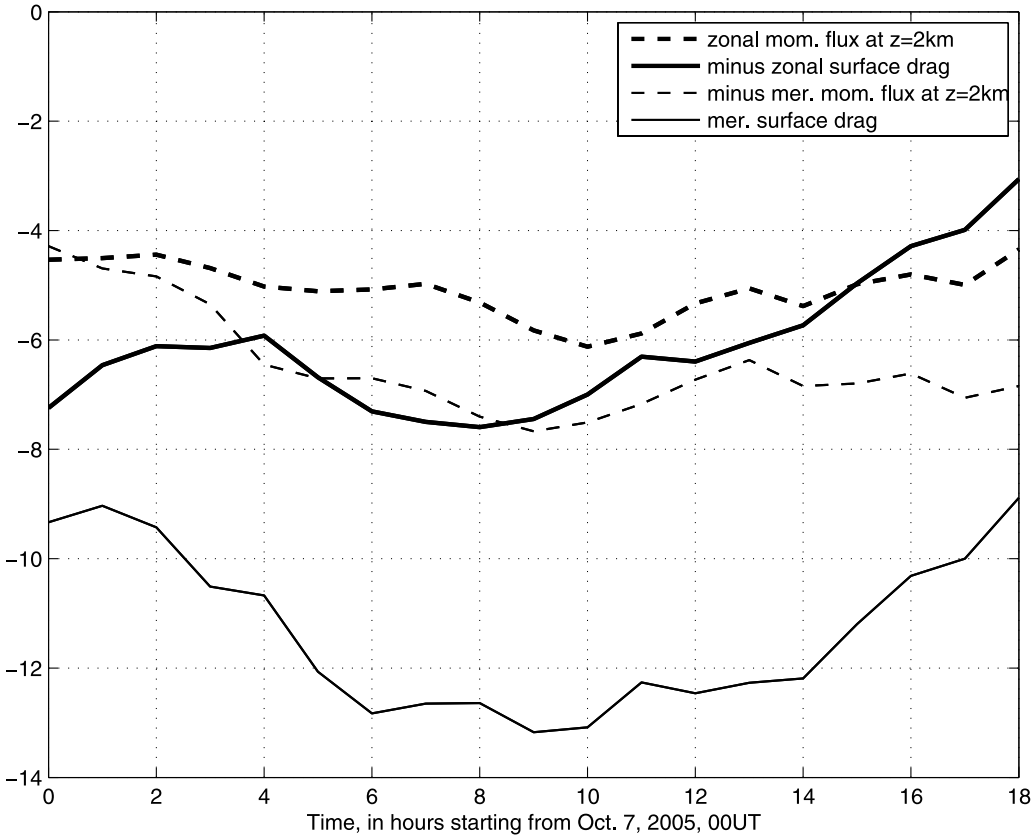

Figure 13. Time evolution of the surface drag and momentum flux at z = 2 km over the region with latitude between 62°S and 65°S, and longitude between 64°W and 54°W, on 7 October 2005, from 0000 UT to 1800 UT. Time is indicated in hours, and drag and momentum flux are indicated in 10^{10} N.

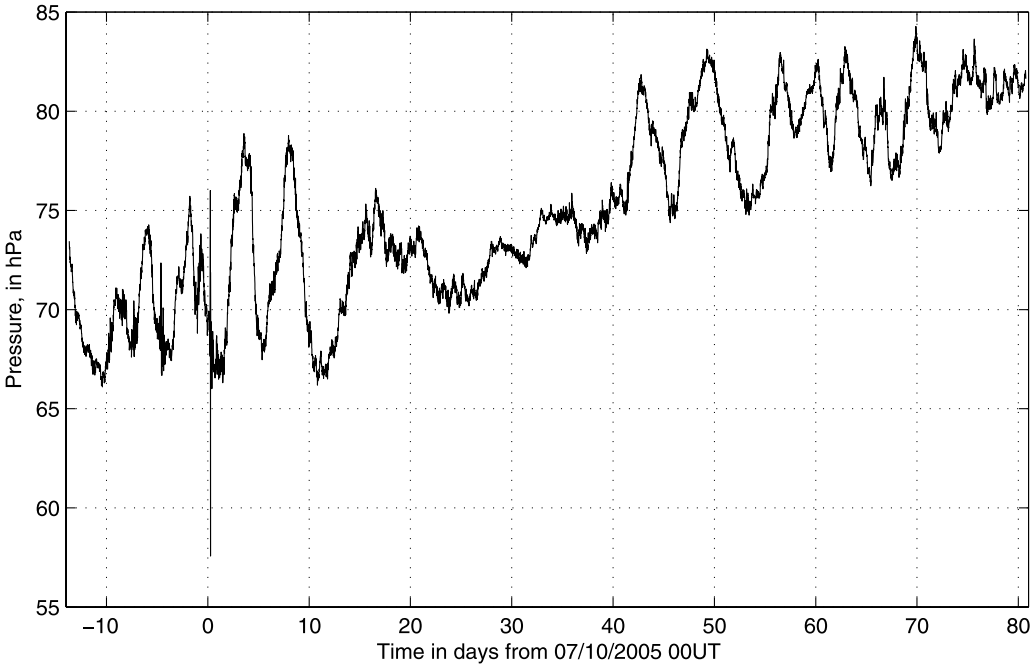

Figure 14. Time series of the pressure for balloon VB11 for the whole of its flight. Time is in days, with the reference time being 7 October, 0000 UT.

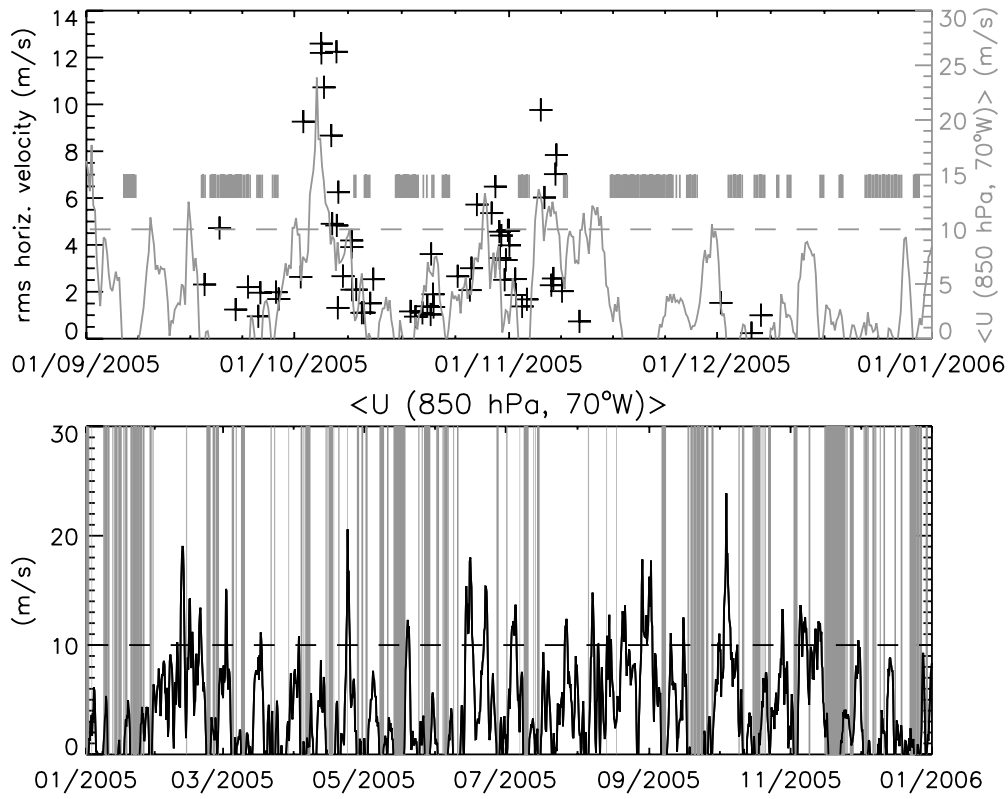

Figure 15. (top) The rms disturbances in horizontal velocities induced by gravity waves above the Antarctic Peninsula estimated from the Vorcore data set (crosses, left scale). The grey curve (right scale) depicts the 850-hPa zonal velocity from the ECMWF operational analyses averaged on a meridional transect (70°W, 62.5–72.5°S) located on the western side of the Antarctic Peninsula. (bottom) The same 850-hPa zonal velocity but for the entire 2005 year. On both panels, the grey shading indicates time periods when the horizontal wind veers by more than 90° in the troposphere in the vicinity of the peninsula, preventing mountain wave propagation into the stratosphere.

appears as a single spike which clearly is an extreme and rare event among the flow situations sampled by the balloon: the pressure jump is 2 orders of magnitude larger than the average pressure jump between successive measurements. Now, the Antarctic Peninsula is known to be a significant source of large-amplitude mountain waves [*Gary*, 1989; *Watanabe et al.*, 2006]. During the Vorcore campaign, several other strong mountain waves were observed by the balloons above the peninsula, but the wave activity in that area appears to be very sporadic [*Hertzog et al.*, 2008]. We propose below a crude estimate of the occurrence of large amplitude mountain waves above the peninsula, which is based on the Vorcore observations and on some knowledge of the large-scale flow upstream of the peninsula.

[45] To this end, we first estimated the mountain wave activity in the vicinity of the Antarctic Peninsula during the Vorcore campaign. Namely, the balloon horizontal velocities were high-pass filtered in order to only deal with disturbances induced by gravity waves. This is easily achieved with long-duration superpressure balloons, as they are almost perfect tracers of horizontal motions. The time series recorded during the balloon flights thus directly exhibit the wave intrinsic frequencies. Accordingly, the cutoff frequency of the filter used to isolate gravity waves was chosen to correspond to the inertial frequency at the latitude of the peninsula. We then defined a geographical area that encompasses the Antarctic Peninsula (55–70°W, 62.5–72.5°S), and we computed the root-mean-square horizontal velocity (i.e., $\sqrt{u'^2 + v'^2}$) associated with each passage of a balloon in that area. The result is displayed (with the crosses) in Figure 15 (top). Figure 15 shows the large variability of gravity wave activity that is observed above the peninsula: background rms amplitudes of GW horizontal velocity disturbances are typically less than 2 m s^{-1}, whereas some wave packets induce disturbances with amplitudes more than 5 time as large (and thus momentum fluxes typically 25 times larger). In particular, the event studied in this article occurred during a time period (early October) which is associated with a larger than usual gravity wave activity. Other similar active periods (though less active) are also observed in late October and early November. Note finally that the observations underestimate the real gravity wave variability in the peninsula area for at least two reasons: first, the observations only provide a limited sampling both in time and space; second, even when a wave is indeed sampled, it is only present in a small portion of the above-mentioned area, so that the rms amplitudes displayed in Figure 15 are smoothed by the averaging.

[46] Figure 15 also shows the analyzed 850-hPa zonal velocity issued by the ECMWF operational system, aver-

aged on the western border of the above-mentioned area. During the Vorcore campaign (Figure 15, top), the periods corresponding to the largest gravity wave activity in the lower stratosphere are mostly associated with a strong zonal velocity in the lower troposphere upstream of the peninsula. This is the expected relation, since the gravity waves observed by the stratospheric balloons in that area are most likely mountain waves generated above the peninsula. Now, we do not expect such a simple correlation to hold perfectly: for instance, the geographical extent of the mountain waves may be smaller than the entire peninsula so that the balloons may miss them on some occasions. Another factor to consider is the possible filtering by tropospheric winds: a further criterion can be considered to identify when the tropospheric winds veer by more than 90°and prevent propagation to the stratosphere, as was done in the analysis of [*Dörnbrack et al.*, 2001]. As seen in Figure 15, this essentially only happens when surface winds are weak or westward. Hence, the waves generated when $u_{850\ \mathrm{hPa}} > 10\ \mathrm{m\ s^{-1}}$ are likely free to propagate to at least 50 hPa and the analyzed 850-hPa zonal velocity is a good proxy for forecasting GW activity in the vicinity of the Antarctic Peninsula: larger wave-induced disturbances are observed when the 850-hPa zonal velocity upstream of the peninsula is typically larger than 10 m s^{-1}. (An equivalent good correlation (not shown) is found between the wave activity in the balloon observations and the time series of gravity wave stress provided by the parameterization implemented in the ECMWF model). If we now consider the whole 2005 year (Figure 15, bottom), about 20 time periods, corresponding to a total of 37 days, are associated with such strong zonal velocities. These periods mostly occur when the propagation conditions for mountain waves throughout the troposphere and into the stratosphere are generally favorable. On the basis of this coarse proxy, we thus expect that GW packets comparable to the one described in this article occur ~10% of the time in the lower stratosphere above the Antarctic Peninsula. It is interesting to note that *Hertzog et al.* [2008] reported very similar values for the intermittency of mountain waves above Antarctica from independent estimations based solely on the Vorcore data set.

5. Conclusion

[47] This study documents the event of a large-amplitude orographic gravity wave observed on 7 October 2005 over the Antarctic Peninsula, using both data and mesoscale model simulations. The data consists principally in measurements from superpressure balloons launched during the Vorcore campaign [*Hertzog et al.*, 2007]. Several balloons were flying in the vicinity of the peninsula at that time, at altitudes between 17 and 19 km (Figure 1), and one of them (VB12) exploded as it was passing over the peninsula.

[48] The observations gathered from the other balloons flying over the peninsula on the same day clearly suggest the presence of a very strong gravity wave above the peninsula. In particular, VB11 flew on a trajectory close to VB12, but about 1.7 km lower and about 4 h earlier. Measurements of pressure, temperature and wind as the balloon flew over the peninsula show very large fluctuations (18 hPa in pressure, 17 K in temperature) which can be interpreted as a gravity wave. However, because the measurements are made only every 15 minutes, the wave is undersampled.

[49] The observations are complemented by numerical simulations with the Weather Research and Forecast model [*Skamarock et al.*, 2005], using two domains with a horizontal resolution of dx = 7 km in the nested domain, and 112 vertical levels up to 1 hPa. The simulations clearly produce a large-amplitude gravity wave above the peninsula. The wave amplitude and characteristics agree with those found and estimated from the observations, as summarized in Table 1. Furthermore, the simulations show that this wave was breaking through static instability in the lower stratosphere on 7 October. This is supported by a radiosounding (section 2.3, Figure 3) just downstream of the mountain, which clearly shows evidence of layers where mixing has occurred in the lower stratosphere.

[50] The simulations were used to obtain estimates of the momentum fluxes associated with the wave. Local values of the momentum fluxes, averaged over boxes 140 km × 140 km, reached 7 to 9 Pa at heights between 15 and 20 km. As the wave is already breaking, the forcing associated with these momentum fluxes will mostly be relevant for the lower stratosphere. Such large amplitude gravity wave events can contribute significantly to climatologies of gravity wave momentum fluxes [*Hertzog et al.*, 2008]. However, it is also essential to estimate their representativity, or in other words their intermittency. From a combined investigation of the Vorcore data and of ECMWF analyses, it was estimated that such large-amplitude gravity wave events are present 10% of the time over the Antarctic Peninsula.

[51] The simulations carried out have also illustrated other impacts of the wave which, in addition to their contribution to momentum fluxes toward the middle atmosphere, can be of importance:

[52] 1. The wave breaking not only leads to a forcing of the mean flow, it also acts as a secondary source of inertia-gravity waves [*Scavuzzo et al.*, 1998; *Fritts et al.*, 2006]. There is evidence of low-frequency inertia-gravity waves in the wake of the breaking region in the lower stratosphere in the simulations (Figures 7 and 11). This is in agreement with the presence of low-frequency oscillations frequently found in the Vorcore data downstream of regions of strong mountain wave packets (not shown).

[53] 2. The breaking of such a wave in the lower stratosphere is a source of clear air turbulence and vertical mixing. Strong evidence for the latter was provided by the radiosounding from Marambio (Figure 3) in which several layers in the lower stratosphere have their potential temperature partially homogenized.

[54] 3. The temperature fluctuations can lead to PSC formation over the peninsula [*Höpfner et al.*, 2006; *Noel et al.*, 2008]. On one hand, the wave induces very large temperature fluctuations (up to 25K), but on the other hand these occur only on short time scales (tens of minutes). In consequence, the impact on microphysics remains unclear.

[55] Further work on several of these issues (intermittency, forcing of secondary waves, identification of nonorographic sources) is underway, again combining Vorcore observations and mesoscale numerical simulations.

[56] **Acknowledgments.** The authors would like to thank the French Space Agency (CNES) for the success of the Vorcore balloon campaign. They also thank IDRIS for the computing resources necessary for these simulations and the LEFE program and the ANR project FLOWINg for financial support. Mohamed Moustaoui is gratefully acknowledged for all of his help with running the WRF model. The authors also wish to thank Lionel Guez for his help with WRF, François Lott for useful indications, and the two referees for their useful comments and suggestions.

References

Alexander, M. J., and T. Dunkerton (1999), A spectral parametrization of mean-flow forcing due to breaking-gravity waves, *J. Atmos. Sci.*, *56*, 4167–4182.

Alexander, M. J., and H. Teitelbaum (2007), Observation and analysis of a large amplitude mountain wave event over the Antarctic peninsula, *J. Geophys. Res.*, *112*, D21103, doi:10.1029/2006JD008368.

Andrews, D., J. Holton, and C. Leovy (1987), *Middle Atmosphere Dynamics*, Academic, Orlando, Fla.

Austin, J., et al. (2003), Uncertainties and assessment of chemistry-climate models of the stratosphere, *Atmos. Chem. Phys.*, *3*, 1–27.

Beau, I., and P. Bougeault (1998), Assessment of gravity-wave drag parameterization with PYREX data, *Q. J. R. Meteorol. Soc.*, *124*, 1443–1464.

Boccara, G., A. Hertzog, R. Vincent, and F. Vial (2008), Estimation of gravity-wave momentum fluxes and phase speeds from long-duration stratospheric balloon flights. 1. Theory and simulations, *J. Atmos. Sci.*, in press.

Broad, A. (1996), High-resolution numerical model integrations to validate gravity-wave-drag parameterization schemes: A case study, *Q. J. R. Meteorol. Soc.*, *122*, 1625–1653.

Bühler, O. (2003), Equatorward propagation of inertia-gravity waves due to steady and intermittent wave sources, *J. Atmos. Sci.*, *60*, 1410–1419.

Buss, S., A. Hertzog, C. Hostettler, T. Bui, D. Lüthi, and H. Wernli (2004), Analysis of a jet stream induced gravity wave associated with an observed ice cloud over Greenland, *Atmos. Chem. Phys.*, *3*, 5875–5918.

Dörnbrack, A., M. Leutbecher, J. Reichardt, A. Behrendt, K.-P. Müller, and G. Baumgarten (2001), Relevance of mountain wave cooling for the formation of polar stratospheric clouds over Scandinavia: Mesoscale dynamics and observations for January 1997, *J. Geophys. Res.*, *106*(D2), 1569–1581.

Dörnbrack, A., T. Birner, A. Fix, H. Flentje, A. Meister, H. Schmid, E. V. Browell, and M. J. Mahoney (2002), Evidence for inertia-gravity waves forming polar stratospheric clouds over Scandinavia, *J. Geophys. Res.*, *107*(D20), 8287, doi:10.1029/2001JD000452.

Fritts, D. C., and M. J. Alexander (2003), Gravity wave dynamics and effects in the middle atmosphere, *Rev. Geophys.*, *41*(1), 1003, doi:10.1029/2001RG000106.

Fritts, D., S. Vadas, K. Wan, and J. Werne (2006), Mean and variable forcing of the middle atmosphere by gravity waves, *J. Atmos. Sol. Terr. Phys.*, *68*(3–5), 247–265.

Gary, B. L. (1989), Observational results using the microwave temperature profiler during the airborne Antarctic ozone experiment, *J. Geophys. Res.*, *94*(D9), 11,223–11,231.

Hamilton, K., R. J. Wilson, J. D. Mahlman, and L. J. Umscheid (1995), Climatology of the SKYHI troposphere-stratosphere-mesosphere general circulation model, *J. Atmos. Sci.*, *52*, 5–43.

Haynes, P. (2005), Stratospheric dynamics, *Annu. Rev. Fluid Mech.*, *37*, 263–293.

Hertzog, A., et al. (2007), Stratéole/Vorcore—Long duration, superpressure balloons to study the Antarctic stratosphere during the 2005 winter, *J. Atmos. Oceanic Technol.*, *24*, 2048–2061.

Hertzog, A., G. Boccara, R. Vincent, F. Vial, and P. Coquerez (2008), Estimation of gravity-wave momentum fluxes and pahse speeds from long-duration stratospheric balloon flights. 2. Results from the Vorcore campaign in Antarctica, *J. Atmos. Sci*, in press.

Holton, J. R. (1992), *An Introduction to Dynamic Meteorology*, 3rd ed., Academic, San Diego, Calif.

Höpfner, M., et al. (2006), MIPAS detects Antarctic stratospheric belt of NAT PSCs caused by mountain waves, *Atmos. Chem. Phys.*, *6*, 1221–1230.

Koch, S., et al. (2005), Turbulence and gravity waves within an upper-level front, *J. Atmos. Sci.*, *62*, 3885–3908.

Lane, T., J. Doyle, R. Plougonven, R. Sharman, and M. Shapiro (2004), Numerical modeling of gravity waves and shearing instabilities above an observed jet, *J. Atmos. Sci.*, *61*, 2692–2706.

Leutbecher, M., and H. Volkert (2000), The propagation of mountain waves into the stratosphere: Quantitative evaluation of three-dimensional simulations, *J. Atmos. Sci.*, *57*, 3090–3108.

Limpasuvan, V., D. Wu, M. J. Alexander, M. Xue, M. Hu, S. Pawson, and J. Perkins (2007), Stratospheric gravity wave simulation over Greenland during 24 January 2005, *J. Geophys. Res.*, *112*, D10115, doi:10.1029/2006JD007823.

Massman, W. J. (1978), On the nature of vertical oscillations of constant volume balloons, *J. Appl. Meteorol.*, *17*, 1351–1356.

Nastrom, G. D. (1980), The response of superpressure balloons to gravity waves, *J. Appl. Meteorol.*, *19*, 1013–1019.

Noel, V., A. Hertzog, H. Chepfer, and D. M. Winker (2008), Polar stratospheric clouds over Antarctica from the CALIPSO spaceborne lidar, *J. Geophys. Res.*, *113*, D02205, doi:10.1029/2007JD008616.

Pawson, S., et al. (2000), The GCM-Reality Intercomparison Project for SPARC (GRIPS): Scientific issues and initial results, *Bull. Am. Meteorol. Soc.*, *81*, 781–796.

Piani, C., W. A. Norton, and D. A. Stainforth (2004), Equatorial stratospheric response to variations in deterministic and stochastic gravity wave parameterizations, *J. Geophys. Res.*, *109*, D14101, doi:10.1029/2004JD004656.

Potter, B., and J. Holton (1995), The role of monsoon convection in the dehydration of the lower tropical stratosphere, *J. Atmos. Sci.*, *52*(8), 1034–1050.

Sato, K. (1994), A statistical study of the structure, saturation and sources of inertio-gravity waves in the lower stratosphere observed with the MU radar, *J. Atmos. Terr. Phys.*, *56*(6), 755–774.

Scavuzzo, C., M. Lamfri, H. Teitelbaum, and F. Lott (1998), A study of the low-frequency inertio-gravity waves observed during the Pyrénées experiment, *J. Geophys. Res.*, *103*(D2), 1747–1758.

Shapiro, J. D. M., Q. Jiang, and D. Bartels (2005), Large-amplitude mountain wave breaking over Greenland, *J. Atmos. Sci.*, *62*, 3106–3126.

Shibata, T., K. Sato, H. Kobayashi, M. Yabuki, and M. Shiobara (2003), Antarctic polar stratospheric clouds under temperature perturbation by nonorographic inertia gravity waves observed by micropulse lidar at Syowa Station, *J. Geophys. Res.*, *108*(D3), 4105, doi:10.1029/2002JD002713.

Skamarock, W., J. Klemp, J. Dudhia, D. Gill, D. Barker, W. Wang, and J. G. Powers (2005), A description of the Advanced Research WRF Version 2, *NCAR Tech. Note, NCAR/TN-468+STR*, Natl. Cent. for Atmos. Res., Boulder, Colo.

Smith, S., J. Doyle, A. Brown, and S. Webster (2006), Sensitivity of resolved mountain drag to model resolution for MAP case-studies, *Q. J. R. Meteorol. Soc.*, *132*, 1467–1487.

Vadas, S., D. Fritts, and M. J. Alexander (2003), Mechanism for the generation of secondary waves in wave breaking regions, *J. Atmos. Sci.*, *60*(1), 194–214.

Vincent, R. A., A. Hertzog, G. Boccara, and F. Vial (2007), Quasi-Lagrangian superpressure balloon measurements of gravity-wave momentum fluxes in the polar stratosphere of both hemispheres, *Geophys. Res. Lett.*, *34*, L19804, doi:10.1029/2007GL031072.

Watanabe, S., K. Sato, and M. Takahashi (2006), A general circulation model study of the orographic waves over Antarctica excited by katabatic winds, *J. Geophys. Res.*, *111*, D18104, doi:10.1029/2005JD006851.

A. Hertzog, Laboratoire de Météorologie Dynamique, École Polytechnique, IPSL, F-91128 Palaiseau, France. (albert.hertzog@lmd.polytecnique.fr)

R. Plougonven and H. Teitelbaum, Laboratoire de Météorologie Dynamique, ENS, IPSL, 24 rue Lhomond, F-75005 Paris, France. (riwal.plougonven@polytechnique.org; teitel@lmd.ens.fr)